HHS Public Access

Author manuscript

J Neurosurg Pediatr. Author manuscript; available in PMC 2018 April 24.

Published in final edited form as:

J Neurosurg Pediatr. 2016 August ; 18(2): 213–223. doi:10.3171/2016.2.PEDS15531.

Toward a better understanding of the cellular basis for cerebrospinal fluid shunt obstruction: report on the construction of a bank of explanted hydrocephalus devices

Brian W. Hanak, MD[1,2], **Emily F. Ross, BA**[1], **Carolyn A. Harris, PhD**[3], **Samuel R. Browd, MD, PhD**[1,2], and **William Shain, PhD**[1,2]

[1]Center for Integrative Brain Research, Seattle Children's Research Institute

[2]Department of Neurological Surgery, University of Washington, Seattle, Washington

[3]Department of Neurosurgery, Wayne State University, Detroit, Michigan

Abstract

OBJECTIVE—Shunt obstruction by cells and/or tissue is the most common cause of shunt failure. Ventricular catheter obstruction alone accounts for more than 50% of shunt failures in pediatric patients. The authors sought to systematically collect explanted ventricular catheters from the Seattle Children's Hospital with a focus on elucidating the cellular mechanisms underlying obstruction.

METHODS—In the operating room, explanted hardware was placed in 4% paraformaldehyde. Weekly, samples were transferred to buffer solution and stored at 4°C. After consent was obtained for their use, catheters were labeled using cell-specific markers for astrocytes (glial fibrillary acidic protein), microglia (ionized calcium-binding adapter molecule 1), and choroid plexus (transthyretin) in conjunction with a nuclear stain (Hoechst). Catheters were mounted in custom polycarbonate imaging chambers. Three-dimensional, multispectral, spinning-disk confocal microscopy was used to image catheter cerebrospinal fluid–intake holes (10× objective, 499.2-μm-thick z-stack, 2.4-μm step size, Olympus IX81 inverted microscope with motorized stage and charge-coupled device camera). Values are reported as the mean ± standard error of the mean and were compared using a 2-tailed Mann-Whitney U-test. Significance was defined at $p < 0.05$.

RESULTS—Thirty-six ventricular catheters have been imaged to date, resulting in the following observations: 1) Astrocytes and microglia are the dominant cell types bound directly to catheter

Correspondence: Brian W. Hanak, Department of Neurological Surgery, University of Washington, Neurosurgery, 325 9th Ave., Seattle, WA 98104. hanakb@uw.edu.

Disclosures

Dr. Browd has ownership in Aqueduct Neurosciences Inc., Aqueduct Critical Care Inc., and Navisonics Inc.

Supplemental Information

Videos

Video 1. https://vimeo.com/154597846.

Author Contributions

Conception and design: Harris, Shain. Acquisition of data: Hanak, Ross. Analysis and interpretation of data: Hanak, Ross. Drafting the article: Hanak. Critically revising the article: Hanak, Harris, Browd, Shain. Reviewed submitted version of manuscript: all authors. Approved the final version of the manuscript on behalf of all authors: Hanak. Administrative/technical/material support: Ross, Harris, Browd. Study supervision: Shain.

surfaces; 2) cellular binding to catheters is ubiquitous even if no grossly visible tissue is apparent; and 3) immunohistochemical techniques are of limited utility when a catheter has been exposed to Bugbee wire electrocautery. Statistical analysis of 24 catheters was performed, after excluding 7 catheters exposed to Bugbee wire cautery, 3 that were poorly fixed, and 2 that demonstrated pronounced autofluorescence. This analysis revealed that catheters with a microglia-dominant cellular response tended to be implanted for shorter durations (24.7 ± 6.7 days) than those with an astrocyte-dominant response (1183 ± 642 days; $p = 0.027$).

CONCLUSIONS—Ventricular catheter occlusion remains a significant source of shunt morbidity in the pediatric population, and given their ability to intimately associate with catheter surfaces, astrocytes and microglia appear to be critical to this pathophysiology. Microglia tend to be the dominant cell type on catheters implanted for less than 2 months, while astrocytes tend to be the most prevalent cell type on catheters implanted for longer time courses and are noted to serve as an interface for the secondary attachment of ependymal cells and choroid plexus.

Keywords

ventriculoperitoneal shunt; shunt failure; shunt obstruction; hydrocephalus; astrocyte; microglia

Hydrocephalus is the abnormal primary accumulation of cerebrospinal fluid (CSF) within the cerebral ventricles resulting from impaired CSF secretion, circulation, or reabsorption. Untreated hydrocephalus generally leads to increased intracranial pressures that can result in neurological damage and even death.[15] In the United States, approximately 1 in 500 individuals has hydrocephalus, and the incidence of congenital hydrocephalus was 5.9 cases per 10,000 persons in a recent population-based retrospective cohort of over 5 million births in the state of California.[9] Hydrocephalus accounts for over 70,000 hospital admissions each year in the United States.[3]

While CSF shunting is the only possible treatment for most cases of hydrocephalus, there have been surprisingly few advances that decrease shunt failure rates since the advent of the Spitz-Holter shunt in the 1950s.[1,2,18] Failure rates today are approximately 40% at 2 years and greater than 90% at 10 years.[4,11,14,19,21] Shunt obstruction by cells or tissue is the most common cause of shunt failure, with ventricular catheter obstruction alone accounting for more than 50% of shunt failures in the pediatric population.[11] Recognizing this, we sought to systematically collect and catalog explanted shunt hardware from the Seattle Children's Hospital (SCH). Our initial focus was to elucidate the cellular mechanisms underlying ventricular catheter obstruction. Here we present our experience in establishing an explanted shunt hardware bank and our initial observations from ventricular catheter imaging.

Methods

Explant Collection

After obtaining approval from the SCH Institutional Review Board (IRB), we commenced the study on April 1, 2013. At the study outset, explanted shunt hardware was collected directly from the operating room at SCH. We received notification from the surgical team at the start of operative cases with the possibility of generating explanted hardware. Explanted hardware was placed in a sterile sputum cup containing 4% paraformaldehyde (PFA) for

transport to our laboratory. In September 2013, the protocol for explant collection was modified, after we obtained approval from the SCH IRB, to allow the surgical team to place explanted hardware in sterile sputum cups containing 4% PFA (which were stored in the operating room for this express purpose) and maintained at room temperature (RT). With this protocol change, explanted shunt hardware samples were collected from the operating room for transport to our laboratory on a weekly basis. Immediately upon arrival to the laboratory, samples were transferred from 4% PFA to HEPES-buffered Hanks solution (HBHS) containing sodium azide (90 mg/L, pH 7.4) and stored at 4°C until processed for imaging.[6]

Obtaining Patient or Parental Consent

Institutional review board–approved consents and Health Insurance Portability and Accountability Act (HIPAA) forms were sent to all patients, or the legal guardians of those, whose explants were collected, along with a cover letter explaining the purpose of study. For patients between the ages of 7 and 13 years, assent forms were also included. If forms were not returned within 2 weeks of mailing, phone calls were made to patients or their legal guardians using an IRB-approved script to determine whether the patient would be taking part in the study and/or to answer any questions pertaining to the study. Once the consent form, HIPAA form, and assent form (if applicable) were obtained, the explant was processed for imaging as described below.

Explant Processing, Staining, and Immunohistochemistry

Explanted ventricular catheters maintained in HBHS containing sodium azide were removed from storage at 4°C and immediately subjected to 3 rapid washes with HBHS containing sodium azide. Catheters were incubated in 5 mg/ml of sodium borohydride in HBHS for 30 minutes at RT to reduce postfixation crosslinking autofluorescence. Next, the catheters were incubated in 0.2% Triton X-100 (Sigma-Aldrich) in HBHS for 30 minutes at RT for cell membrane permeation to permit antibody penetration to intracellular sites. Catheters were then incubated in ImageiT FX signal enhancer (Invitrogen, Thermo Fisher Scientific) for 30 minutes at RT to prevent nonspecific labeling.

Catheters were labeled with 1:1000 monoclonal rat anti–glial fibrillary acidic protein (GFAP; astrocyte marker, Invitrogen), 1:800 monoclonal rabbit anti–ionized calcium-binding adapter molecule 1 (Iba-1; microglia marker, Wako Pure Chemical Industries), and 1:1000 polyclonal chicken anti-transthyretin (TTR; choroid plexus marker, Pierce Antibodies, Thermo Fisher Scientific) for 24 hours at RT. Subsequently, 1:200 goat anti–rat Alexa Fluor 488, 1:200 goat anti–rabbit Alexa Flour 594, and 1:200 goat anti–chicken Alexa Flour 647 (all Invitrogen) conjugated secondary antibodies were applied for 24 hours at RT. Additionally, at the time of secondary antibody application, catheters were stained with 1:1000 Hoechst (Sigma-Aldrich) for the identification of cell nuclei.

After 24 hours in secondary antibodies and Hoechst, the catheters were washed 4 times over 30 minutes with HBHS containing sodium azide and 0.5% TWEEN 20 (Sigma-Aldrich). Lastly, the ventricular catheters were mounted using Fluoromount-G (SouthernBiotech) in custom polycarbonate imaging chambers, which allowed for the application of cover slips to

both sides of the chamber (for ease of imaging CSF intake holes oriented on opposite sides of the catheter).

Explant Imaging

Three-dimensional, multispectral, spinning-disk confocal microscopy was used to image explanted ventricular catheters (Olympus IX81 inverted microscope with motorized x-y-z stage, broad-spectrum light source, and chargecoupled device camera). Confocal images (800 × 800 × 499.2 μm) in and around catheter CSF-intake holes were acquired using a 10× objective (209 optical z-sections, 2.4- μm step size). For all catheters included in the study, at least one-half of all CSF intake holes (range 10–20) were imaged using this method. Additionally, the external surface of all catheters was reviewed using wide-field fluorescence microscopy, and representative confocal images of cells attached or extending from the surface of the catheter were also obtained. For transparent catheters, representative images of cell masses attached to the luminal surface were also obtained. In select cases in which cellular material within the depth of a CSF intake hole or within the catheter lumen could not be adequately imaged through the holes themselves, the catheter would be sectioned using a scalpel blade No. 10, allowing for a cross-sectional view of the CSF intake hole edges. Note that catheter manipulation or sectioning was performed only after completing standardized systematic imaging of the catheter CSF-intake holes and outer surfaces.

Clinical Data Collection

Clinical and patient data associated with each imaged catheter was reviewed in a retrospective fashion including patient age at the time of catheter removal, length of time the catheter was implanted, etiology of the patient's hydrocephalus, and catheter make. Additionally, a retrospective review of all operative cases treated at SCH for the management of hydrocephalus between the start of the shunt explant bank on April 1, 2013, and November 30, 2014, was performed using operative billing records for the primary purpose of assessing explant accrual rates.

Statistics

Discrete nonparametric variables (for example, patient age, period of catheter implantation) are reported as the mean ± standard error of the mean and were compared using a 2-tailed Mann-Whitney U-test. Statistical analysis was performed using the Statistical Package for the Social Sciences version 20.0 (IBM Corp.). Statistical significance was defined at $p < 0.05$.

Results

Sample Accrual and Clinical Data

Between April 1, 2013, and November 30, 2014, 211 patients underwent operative intervention for hydrocephalus management at SCH (Table 1). The etiology of the hydrocephalus for each patient was determined by chart review, with intraventricular hemorrhage of prematurity (23.2%), tumor (19.9%), and myelomeningocele (17.1%) representing the most common etiologies in the patient population as a whole (Table 2). There were 221 shunt revision surgeries during the study period. The primary indication for

shunt revision surgery was acute shunt malfunction symptomology (81.0%), with presumed shunt infection (14.0%), asymptomatic hardware discontinuities (3.6%), and overdrainage symptoms (1.4%) accounting for the remainder of the preoperative indications for intervention (Table 3). A total of 122 patients presented with acute shunt malfunction on 179 occasions, and 85.2% of these patients demonstrated an increased ventricular size on preoperative cranial imaging when they presented with acute malfunction (while the remainder had a stable ventricular size). Intraoperative findings demonstrated that ventricular catheter obstruction was the leading confirmed cause of ventriculoperitoneal (VP) shunt failure, noted in 81 (53.6%) of 151 cases (Table 4).

Overall, including proximal catheters, external ventriculostomy drains, valves, and distal catheters, 321 surgeries resulted in the removal of shunt hardware. We received hardware in 34.0% (109/321) of cases. As hospital staff became increasingly comfortable with the protocol, our accrual rates improved, with increasing accrual rates by progressive study trimesters: 13.8% (15/109), 39.6% (40/101), and 48.6% (54/111). Figure 1 displays the number of surgeries resulting in explanted hardware as well as the number of samples collected on a month-by-month basis. Consent was obtained for 46 (58.2%) of the 79 ventricular catheters received. Twelve (26.1%) of the 46 consented catheter samples were removed using a Bugbee wire (monopolar electrocautery).

Explant Imaging

Thirty-six ventricular catheters have been systematically imaged to date, and this initial experience has yielded several noteworthy findings. First, cell attachment to ventricular catheters is ubiquitous even if no grossly visible tissue is apparent to the naked eye (Fig. 2), although the distribution of cells along the catheter surface is anything but homogeneous. All imaged catheters demonstrated a relative paucity of cells on the outer catheter surface with much more robust cell attachment to the CSF intake holes and lumen.

Statistical analysis was performed on 24 of the 36 imaged catheters (Table 5). Documented exposure to Bugbee wire monopolar electrocautery at the time of explantation was the most common reason for exclusion from analysis (7 catheters; Table 6). Ventricular catheters exposed to Bugbee wire electrocautery were processed with immunohistochemical (IHC) labeling in a manner identical to their noncauterized counterparts; however, all imaged Bugbee wire–exposed catheters demonstrated at least some degree of IHC fluorescence signal loss, particularly within the catheter lumen and in the depths of the CSF intake holes, presumably because of more pronounced protein denaturation and therefore loss of immunoreactivity at these sites. Figure 3 demonstrates a cluster of astrocytes extending from a point of attachment to the CSF intake hole of a Bugbee wire–exposed catheter. Note that the relative lack of well-defined immunofluorescent signal within the confines of the CSF intake hole blends smoothly with the robust GFAP labeling of the appendage-like cell mass that extends from the hole, demonstrating the “Bugbee wire effect.” Although the primary observed cellular response is noted for Bugbee wire–exposed catheters in Table 6, these catheters were not included in statistical analysis given our concern that the data associated with these catheters are, at the very least, incomplete given the loss of tissue or immunoreactivity and may be erroneous given the potential for altered IHC labeling in the

context of protein denaturation. Additionally, 5 catheters not treated with Bugbee wires were excluded from statistical analysis because of either pronounced autofluorescence (2 catheters, both barium impregnated), which precluded analysis of critical fluorescence channels, or weak and/or irregular IHC labeling (3 catheters) attributed to poor, inadequate, or excessive fixation versus undocumented Bugbee exposure versus errors in sample preparation.

The 24 catheters included in our analysis afford insight into the cell types directly bound to the poly(dimethylsiloxane) (PDMS) catheter surfaces. In all 24 samples imaged, the majority of cells in direct contact with the PDMS catheter surfaces were either astrocytes or of the macrophage lineage (presumptively microglia) based on the presence of GFAP or Iba-1 immunoreactivity, respectively. In addition to their unique propensity to intimately associate with the PDMS catheter surfaces, astrocytes and microglia are the most abundant cell types observed overall when imaging catheter CSF-intake holes. All CSF intake holes within a given catheter demonstrated similar patterns of cell attachment, allowing for qualitative classification of each imaged catheter as possessing an astrocyte-dominant, microglia-dominant, or mixed (astrocyte and microglia) response. Figure 4 demonstrates representative images of these three observed cellular responses.

Six catheters (25%) demonstrated sparse GFAP/Iba-1 double-negative cell masses with punctate TTR labeling most likely representing sloughed ependymal cells[13] versus small clusters of choroid plexus (Fig. 5). In all 6 cases, these TTR-positive cells were noted to be secondarily attached to underlying masses of astrocytes and were only observed in a subset of imaged catheter holes (range 5%–31%). One catheter was noted to have gross choroid plexus attachment (Fig. 6 and Video 1).

Three-dimensional confocal imaging revealed that the choroid plexus affixed to the CSF intake holes of the catheter was not directly bound to the PDMS catheter surface but rather was attached secondarily via networks of astrocytes, which were more intimately associated with the catheter surface. Note that this catheter's overall cellular response was graded as "mixed" given significant clusters of microglia interfacing with the catheter surface in CSF intake holes without the dramatic secondary choroid plexus attachment shown in Fig. 6.

The observed cellular responses were related to the length of time the catheter was implanted, with microglia-dominant responses occurring on catheters implanted for shorter durations (24.7 ± 6.7 days) than the catheters with astrocyte-dominant responses (1183 ± 642 days; $p = 0.027$). Mixed responses were generally observed on catheters implanted for an intermediate length of time (51.5 ± 15.3 days; $p = 0.37$, compared with microglia dominant; $p = 0.073$, compared with astrocyte dominant). A trend was noted with respect to patient age, with microglia-dominant responses generally occurring in younger patients (28.3 ± 16.7 months) and mixed and astrocyte-dominant responses in older patients (97.0 ± 26.5 and 92.5 ± 38.7 months, respectively); however, these differences were not statistically significant ($p = 0.061$, comparing microglia-dominant with mixed/astrocyte-dominant responses). The study was not sufficiently powered to attempt to correlate the observed cellular response with factors such as the patient's hydrocephalus etiology or the type of catheter implanted, and thus far no striking patterns have emerged with respect to

these variables (Table 5). Note that the greater variability in catheter models among those catheters demonstrating astrocyte-dominant responses is probably a reflection of the longer implantation periods associated with this response (that is, increased temporal variability in practice standards with respect to implant choice).

Discussion

This study presents our initial experience in establishing an explanted shunt hardware bank and systematically imaging ventricular catheters with 3D confocal microscopy. This work has yielded several observations that expand upon prior investigations of cell-shunt interactions: 1) cellular binding to ventricular catheters is ubiquitous even if no grossly visible tissue is apparent; 2) IHC techniques are often of limited utility when a ventricular catheter has been exposed to Bugbee wire monopolar electrocautery because of the associated protein denaturation or loss of immunoreactivity; 3) astrocytes and microglia are the dominant cell types bound directly to the PDMS surfaces of ventricular catheters and therefore appear to be of paramount importance in the pathophysiology of shunt occlusion; and 4) the length of time a catheter has been implanted correlates with the dominant cell type observed, with microglia-dominant responses occurring on catheters implanted for shorter time periods and astrocyte-dominant responses occurring on catheters implanted for longer time periods.

Although contrary to early investigations of noninfectious ventricular catheter occlusion[8] and neurosurgical lore, which has long held choroid plexus to be the main culprit behind catheter obstructions, our finding that astrocytes and microglia are the primary cell types responsible for ventricular catheter occlusion agrees with more recent work in the field. Notably, a 2014 publication by Sarkiss et al.,[20] who investigated obstructive luminal material in 85 explanted ventricular catheters using modern clinical pathology techniques (IHC, light microscopy), demonstrated that choroid plexus luminal obstructions were a relatively rare finding (7% overall). The present study expands on this work by demonstrating that astrocytes and microglia are not only the most abundant cell types present on explanted ventricular catheters but also appear to be uniquely capable of adhering to the PDMS catheter surface, implying that they are critical to the pathogenesis of obstructive shunt failure. The finding of attached cells on all explanted catheters in our study, even those with no grossly visible tissue, may partially explain the historical bias in the literature toward choroid plexus being chiefly responsible for catheter obstructions. As choroid plexus is the only macroscopically visible tissue that can be seen on explanted devices, selective study of explanted catheters possessing adherent tissue obvious to the operating surgeon would certainly overemphasize the importance of choroid plexus in the pathogenesis of shunt obstruction.

Our approach to studying ventricular catheter–cell interactions has 2 major advantages over prior work in the field. First, it allows for preservation of the catheter structure (as well as attached cells or tissue) during processing or imaging. Prior studies relying on traditional pathological analysis techniques have required longitudinally cutting the catheter to image retained cells or tissue using traditional light microscopy techniques.[20,22] Moreover, the use of dehydration techniques required for paraffin embedding of samples leads to the

contraction of cells or tissue but does not alter the PDMS catheter dimensions, resulting in an inability to assess the cell-catheter interface.[20] Similarly, studies utilizing scanning electron microscopy have generally employed catheter dissection to visualize CSF intake holes and luminal surfaces because of the need to expose these surfaces for sputter coating prior to imaging.[7,23] Second, by utilizing 3D confocal microscopy for catheter imaging, we are able to comment not only on what cell types are present but also on their 3D relationship to one another and to catheter surfaces. Central to our hypothesis that astrocytes and microglia are primarily responsible for ventricular catheter obstructions is the finding that these cell types are consistently and uniquely bound directly to the PDMS surface of explanted ventricular catheters, particularly at CSF intake holes. Moreover, the observation that choroid plexus and ependymal cells, when present, are always attached to the catheter secondarily via an astrocyte “bridge” is a novel observation that may explain why choroid plexus attachment tends not to be an issue for catheters implanted less than 2 months, such as external ventriculostomy drains. Elucidating the mechanisms by which astrocytes migrate to or proliferate on the surface of implanted catheters will probably provide insight into approaches for reducing late (> 2 months) shunt failure.

The fact that attached astrocytes and microglia were present on the surfaces of all explanted catheters suggests that activation of the innate repair and immune responses of the CNS, either secondary to the persistent presence of a foreign body (the catheter) or secondary to tissue injury with catheter placement, is the most likely inciting event. The observed correlation between catheter implantation time and observed cellular response suggests a stepwise process whereby microglia are the first cells to associate with the catheter surface. This notion is consistent with the knowledge that microglia are highly motile in vivo,[17,24] particularly after tissue injury[5,12] as would occur with catheter insertion through brain parenchyma. The migration of astrocytes onto the catheter surface appears to occur over a longer time course. It remains unknown whether the temporal correlations observed reflect microglia recruitment of parenchymal astrocytes via cytokine signaling, differences in cellular motility, or yet unconsidered mechanisms. While we posit that the Iba-1–positive cells observed on catheter surfaces are parenchymal in origin, one may question whether some of the Iba-1–positive cells observed on the catheters could have originated from choroid plexus, which is known to harbor Iba-1–positive macrophages. [10] Given the lack of GFAP expression in choroid plexus,[16] however, the astrocytes observed on catheters can be more definitively classified as parenchymal in origin.

The finding that catheters removed with the use of intraoperative Bugbee wire monopolar electrocautery demonstrate scant or irregular IHC labeling at CSF intake holes is certainly not surprising as protein denaturation and associated destruction of immunoreactive sites are to be expected with the use of this technique. The return of normal IHC labeling at a distance (range 0.1–2.0 mm) from CSF intake holes in Bubgee wire–treated samples is consistent with expected electrical current dispersion, and the variable distance for the return of typical IHC labeling probably reflects variability in Bugbee wire power settings and duration of current application. The Bugbee wire effect is presented in this report to highlight the limitations of IHC techniques in studying explanted catheters and to alert researchers in the field who may be less familiar with operative neurosurgical techniques in the use of this device. Additionally, it should be noted that choroid plexus remains the most

likely cause of resistance to catheter removal, which would prompt the use of a Bugbee wire, thus potentially resulting in an underrepresentation of samples containing significant amounts of attached choroid. Notably, all Bugbee wire–treated catheters had been implanted for more than 3 months and possessed evidence of astrocyte attachment, consistent with observations made in the non–Bugbee wire–treated group. It is also conceivable that choroid plexus is sometimes avulsed from the catheter surface at the time of catheter explantation even in the absence of Bugbee wire use.

The present study is primarily intended to demonstrate the feasibility of maintaining a prospective shunt explant bank while highlighting preliminary observations. These initial observations certainly warrant more exhaustive follow-up, and this work is ongoing. Further studies should include an even broader panel of cell markers. For instance, while the presence of ependymal cells could be inferred in GFAP- and Iba-1–negative cells with punctate TTR labeling,[13] more specific markers for ependyma, such as myosin VIIa,[25] were not used in the present study. Moreover, cell types observed sporadically in prior studies of noninfectious ventricular catheter obstruction, including lymphocytes, multinucleated giant cells, “connective tissue”/fibroblasts, and leptomeninges/mesothelial cells, were not specifically labeled.[20,22,23] Given the absence of unlabeled cell masses in our initial study, we are inclined to think that the role of these sporadically observed cell types is relatively limited, but further confirmation of this hypothesis is certainly warranted.

Our review of clinical data highlights the challenge of attempting to modify the routine of a well-established surgical team via the introduction of a new research protocol, as evidenced by initially poor explant accrual rates in the early months of the study. Additionally, consistent with prior studies,[11] our review of clinical data at SCH demonstrates that isolated ventricular catheter obstruction accounts for more than half of all VP shunt failures in the pediatric hydrocephalus population, further underscoring the value of pursuing a better understanding of the cellular mechanisms at play to guide the development of next-generation, obstruction-resistant ventricular catheters.

Conclusions

This study shows the feasibility of creating a catalog of explanted hydrocephalus shunt hardware for the purpose of better understanding the cellular mechanisms underlying shunt failure. Initial observations from explanted ventricular catheter imaging highlight the importance of the astrocyte- and microglia-mediated cellular responses to implanted CNS devices in precipitating shunt failure and provide evidence to debunk the notion that choroid plexus infiltration is the primary driver of ventricular catheter occlusions. Primarily microglia-mediated cellular responses to ventricular catheters tend to be seen in devices implanted for shorter periods of time, whereas astrocyte-dominant responses are seen in catheters implanted for longer durations (generally more than 2 months). The mechanisms underlying this temporal progression remain unknown and warrant further study.

Supplementary Material

Refer to Web version on PubMed Central for supplementary material.

Abbreviations

CSF	cerebrospinal fluid
GFAP	glial fibrillary acidic protein
HBHS	HEPES-buffered Hanks solution
HIPAA	Health Insurance Portability and Accountability Act
IHC	immunohistochemical
IRB	institutional review board
PDMS	poly(dimethylsiloxane)
PFA	paraformaldehyde
RT	room temperature
SCH	Seattle Children's Hospital
TTR	transthyretin

References

1. Aschoff A, Kremer P, Hashemi B, Kunze S. The scientific history of hydrocephalus and its treatment. Neurosurg Rev. 1999; 22:67–95. [PubMed: 10547004]
2. Baru JS, Bloom DA, Muraszko K, Koop CE. John Holter's shunt. J Am Coll Surg. 2001; 192:79–85. [PubMed: 11192928]
3. Bondurant CP, Jimenez DF. Epidemiology of cerebrospinal fluid shunting. Pediatr Neurosurg. 1995; 23:254–259. [PubMed: 8688350]
4. Browd SR, Ragel BT, Gottfried ON, Kestle JR. Failure of cerebrospinal fluid shunts: part I: Obstruction and mechanical failure. Pediatr Neurol. 2006; 34:83–92. [PubMed: 16458818]
5. Davalos D, Grutzendler J, Yang G, Kim JV, Zuo Y, Jung S, et al. ATP mediates rapid microglial response to local brain injury in vivo. Nat Neurosci. 2005; 8:752–758. [PubMed: 15895084]
6. Gage GJ, Kipke DR, Shain W. Whole animal perfusion fixation for rodents. J Vis Exp. 2012; 65:3564.
7. Gower DJ, Lewis JC, Kelly DL Jr. Sterile shunt malfunction. A scanning electron microscopic perspective. J Neurosurg. 1984; 61:1079–1084. [PubMed: 6502236]
8. Hakim S. Observations on the physiopathology of the CSF pulse and prevention of ventricular catheter obstruction in valve shunts. Dev Med Child Neurol Suppl. 1969; 20:42–48. [PubMed: 5263250]
9. Jeng S, Gupta N, Wrensch M, Zhao S, Wu YW. Prevalence of congenital hydrocephalus in California, 1991–2000. Pediatr Neurol. 2011; 45:67–71. [PubMed: 21763944]
10. Katsumoto A, Lu H, Miranda AS, Ransohoff RM. Ontogeny and functions of central nervous system macrophages. J Immunol. 2014; 193:2615–2621. [PubMed: 25193935]
11. Kestle J, Drake J, Milner R, Sainte-Rose C, Cinalli G, Boop F, et al. Long-term follow-up data from the Shunt Design Trial. Pediatr Neurosurg. 2000; 33:230–236. [PubMed: 11155058]
12. Kim JV, Dustin ML. Innate response to focal necrotic injury inside the blood-brain barrier. J Immunol. 2006; 177:5269–5277. [PubMed: 17015712]
13. Kuchler-Bopp S, Ittel ME, Dietrich JB, Reeber A, Zaepfel M, Delaunoy JP. The presence of transthyretin in rat ependymal cells is due to endocytosis and not synthesis. Brain Res. 1998; 793:219–230. [PubMed: 9630636]

14. Lutz BR, Venkataraman P, Browd SR. New and improved ways to treat hydrocephalus: Pursuit of a smart shunt. Surg Neurol Int. 2013; 4(Suppl 1):S38–S50. [PubMed: 23653889]
15. McAllister JP II, Williams MA, Walker ML, Kestle JR, Relkin NR, Anderson AM, et al. An update on research priorities in hydrocephalus: overview of the third National Institutes of Health-sponsored symposium "Opportunities for Hydrocephalus Research: Pathways to Better Outcomes. J Neurosurg. 2015; 123:1427–1438. [PubMed: 26090833]
16. Miettinen M, Clark R, Virtanen I. Intermediate filament proteins in choroid plexus and ependyma and their tumors. Am J Pathol. 1986; 123:231–240. [PubMed: 2422943]
17. Nimmerjahn A, Kirchhoff F, Helmchen F. Resting microglial cells are highly dynamic surveillants of brain parenchyma in vivo. Science. 2005; 308:1314–1318. [PubMed: 15831717]
18. Nulsen FE, Spitz EB. Treatment of hydrocephalus by direct shunt from ventricle to jugular vain. Surg Forum. 1951; 1951:399–403.
19. Pollack IF, Albright AL, Adelson PD. A randomized, controlled study of a programmable shunt valve versus a conventional valve for patients with hydrocephalus. Neurosurgery. 1999; 45:1399–1411. [PubMed: 10598708]
20. Sarkiss CA, Sarkar R, Yong W, Lazareff JA. Time dependent pattern of cellular characteristics causing ventriculoperitoneal shunt failure in children. Clin Neurol Neurosurg. 2014; 127:30–32. [PubMed: 25459240]
21. Scott RM, Madsen JR. Shunt technology: contemporary concepts and prospects. Clin Neurosurg. 2003; 50:256–267. [PubMed: 14677444]
22. Sekhar LN, Moossy J, Guthkelch AN. Malfunctioning ventriculoperitoneal shunts. Clinical and pathological features. J Neurosurg. 1982; 56:411–416. [PubMed: 7057239]
23. Takahashi Y, Ohkura A, Hirohata M, Tokutomi T, Shigemori M. Ultrastructure of obstructive tissue in malfunctioning ventricular catheters without infection. Neurol Med Chir (Tokyo). 1998; 38:399–404. [PubMed: 9745244]
24. Wake H, Moorhouse AJ, Jinno S, Kohsaka S, Nabekura J. Resting microglia directly monitor the functional state of synapses in vivo and determine the fate of ischemic terminals. J Neurosci. 2009; 29:3974–3980. [PubMed: 19339593]
25. Wei D, Levic S, Nie L, Gao WQ, Petit C, Jones EG, et al. Cells of adult brain germinal zone have properties akin to hair cells and can be used to replace inner ear sensory cells after damage. Proc Natl Acad Sci U S A. 2008; 105:21000–21005. [PubMed: 19064919]

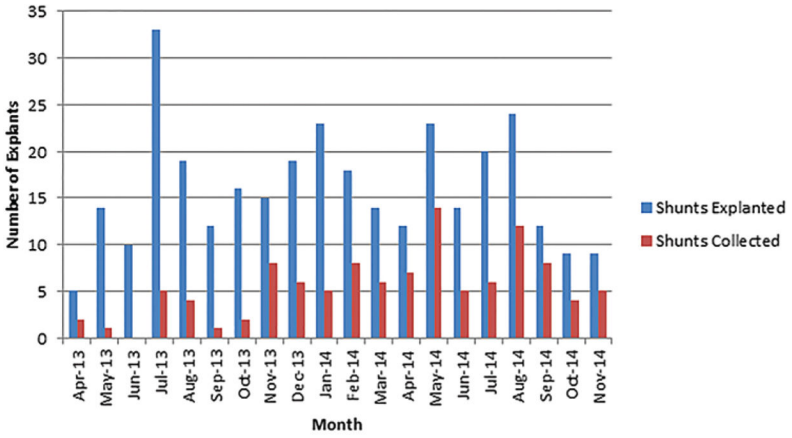

FIG. 1.

Graph showing number of operative cases resulting in explanted hardware per month compared with hardware included in study. Figure is available in color online only.

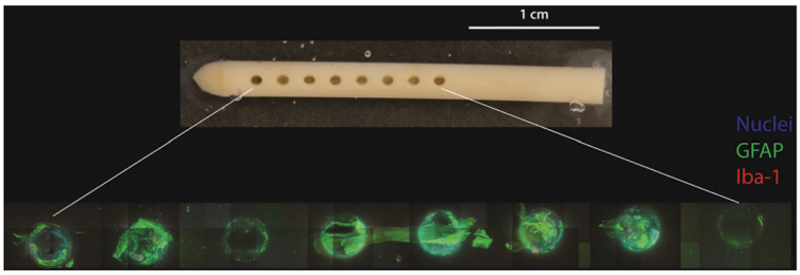

FIG. 2.

Gross photograph of explanted Medtronic Ares antibiotic-impregnated catheter (**upper**) alongside 10× images of the same CSF intake holes (**lower**). Note the presence of a robust astrocyte-dominant response (*green*) by microscopic examination as well as the relative paucity of attached cells on the surfaces between the CSF intake holes. All images obtained with 499.2-μm z-stack, 2.4-μm step size. Figure is available in color online only.

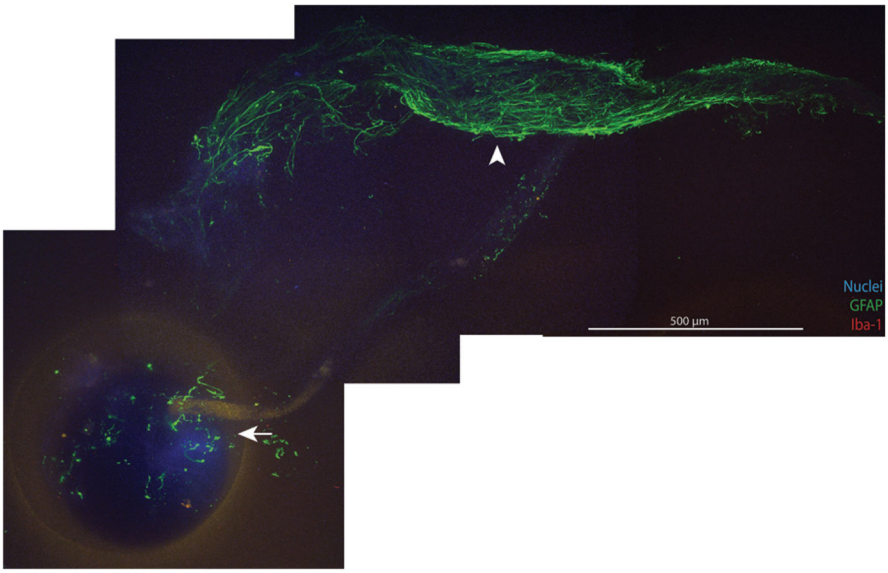

FIG. 3.

Montage of images of a Bugbee wire–exposed catheter demonstrating scant or irregular IHC labeling within the lumen and CSF intake holes (*arrow*). Cell masses demonstrate the return of typical immunoreactivity beyond a variable distance (range 0.1–2.0 mm) from the CSF intake hole (*arrowhead*). All images obtained with 10× objective, 499.2-µm z-stack, 2.4-µm step size. Figure is available in color online only.

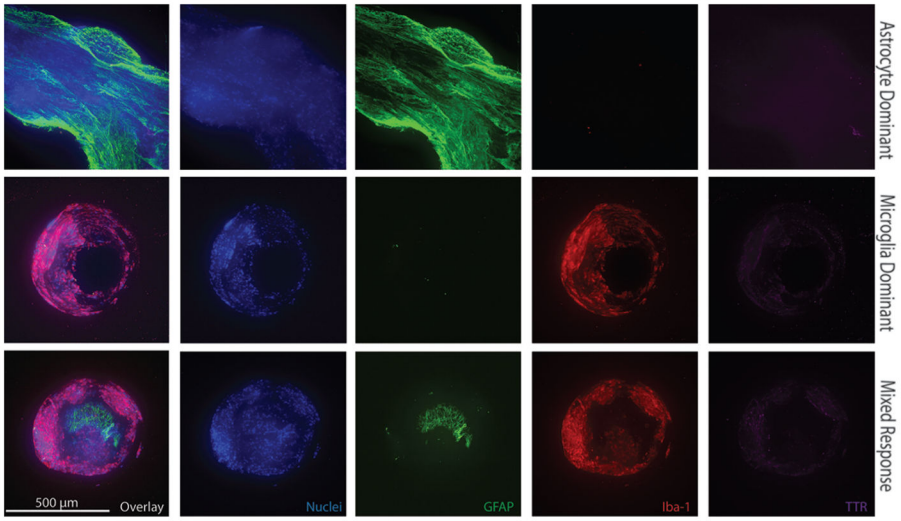

FIG. 4.

Immunohistochemical images of individual CSF intake holes from 3 different explanted ventricular catheters demonstrating representative astrocyte-dominant, microglia-dominant, and mixed responses. All images obtained with 10× objective, 499.2-µm z-stack, 2.4-µm step size. Figure is available in color online only.

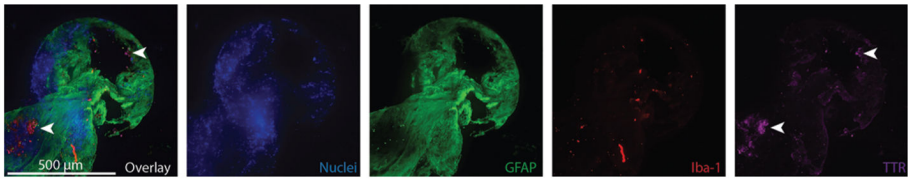

FIG. 5.

Immunohistochemical images of a CSF intake hole that demonstrate an astrocyte-dominant response (*green*). Peripherally bound to the astrocyte cell mass are cells demonstrating punctate TTR (*purple*) labeling in the absence of GFAP or Iba-1 labeling, which are presumed to be sloughed ependymal cells (*arrowheads*). 10× objective, 499.2-μm z-stack, 2.4-μm step size. Figure is available in color online only.

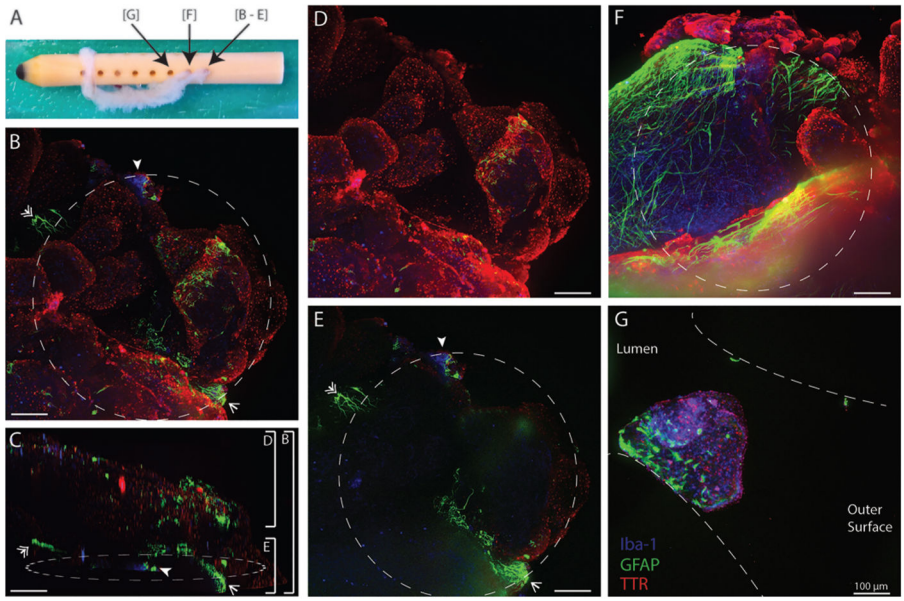

FIG. 6.

A Medtronic Ares antibiotic-impregnated catheter demonstrating extensive choroid plexus attachment via an interface with astrocytes and microglia directly bound to the catheter surface. **A:** In the gross photograph of the explanted catheter, choroid plexus can be seen attached to the 2 most distal CSF intake holes. The attached choroid plexus was wrapped around the catheter near the most proximal CSF intake hole when it was received from the operating room, but during catheter processing it became clear that there was no point of fixation securing it in that position. *Arrows* indicate which hole is being imaged in the subsequent figure panels. **B:** A maximum projection 10× field (408-µm z-stack, 2.4-µm step size) of the distal-most CSF intake hole. The edges of the CSF intake hole were identified by means of bright-field imaging and are indicated by a *dashed white line*. Note the presence of clusters of astrocytes (*arrow* and *double arrow*) as well as a mixed cluster of microglia and astrocytes (*arrowhead*) at the perimeter of the CSF intake hole. **C:** To better appreciate the nature of the cell-catheter interface, the entire maximum projection from panel B has been vertically rotated 84°, as has the *dashed white line* denoting the CSF intake hole edges. The low resolution of the rotated 3D projection reflects decreased resolution in the z-dimension (2.4-µm/pixel as opposed to 0.8-µm/pixel in the x-y plane). Video 1 demonstrates this 3D rotation as an 8.4-second movie. The *white brackets* on the right of the panel denote the selected portions of the z-stack presented as maximum projections in panels B, D, and E. The *arrow*, *double arrow*, and *arrowhead* denote the same astrocyte and microglia/astrocyte clusters highlighted in panel B. **D:** A maximum projection of 100 z-stacks (237.6-µm) above the confines of the CSF intake hole, allowing for visualization of the choroid plexus (*red*) morphology. Note the presence of some astrocytes (*green*) attached to the surface of the lobule of choroid at the 3 o'clock position. **E:** A maximum projection of the 51 z-stacks (120.0-µm) at the CSF intake hole interface. Note that at the interface with the catheter surface, astrocytes (*green*) and, to a lesser extent in this case, microglia (*blue*) predominate, with the 2 astrocyte clusters (*arrow* and *double arrow*) and 1 mixed microglia/astrocyte cluster (*arrowhead*) appearing to serve as points of choroid plexus (*red*) fixation to the

catheter. **F:** A maximum projection 10× field (499.2-μm z-stack, 2.4-μm step size) of the second most distal CSF intake hole demonstrating an extensive mesh of astrocytes (*green*) at the CSF intake hole interface, which extends onto the large mass of choroid plexus (*red*) above the confines of the CSF intake hole (3–7 o'clock positions; hole edges denoted by *dashed white line*). A cuff of choroid is seen to extend just outside the confines of the CSF intake hole (11–3 o'clock positions). **G:** Although not macroscopically visible in panel A, a small piece of choroid plexus (*red*) was noted at the time of catheter imaging within the depths of the third most distal CSF intake hole. Given its depth within the hole, the catheter had to be sectioned to completely visualize the interface between the mass of choroid plexus and the catheter surface. The *dashed white lines* denote the cross-sectioned boundaries of the CSF intake hole. Note that again astrocytes predominate at the interface with the catheter surface. Maximum projection, 10× objective, 360-μm z-stack, 2.4-μm step size. Figure is available in color online only.

TABLE 1

Demographics of the patient population with hydrocephalus at SCH*

Variable	Overall Value	Value by Sex: Male/Female
No. of patients (%)	211	122 (57.82%)/89 (42.18%)
Mean age in yrs	6.89 ± 6.26	6.72 ± 6.10/7.12 ± 6.48
Total no. of surgeries	474	272/202
Mean no. of surgeries per patient	2.25 ± 2.21	2.23 ± 1.89/2.27 ± 2.60

*Values expressed as the mean ± standard deviation unless indicated otherwise.

TABLE 2

Summary of hydrocephalus etiologies in the SCH population of 211 patients

Etiology	No. of Patients (%)	Patient Sex: M (%)/F (%)	Average Patient Age (yrs)
Intraventricular hemorrhage of prematurity	49 (23.22)	22 (18.03)/27 (30.34)	6.25
Brain tumor	42 (19.91)	25 (20.49)/17 (19.10)	8.17
Myelomeningocele	36 (17.06)	26 (21.31)/10 (11.24)	5.08
Aqueductal stenosis	18 (8.53)	11 (9.02)/7 (7.87)	7.92
Congenital CNS malformation	17 (8.06)	9 (7.38)/8 (8.99)	7.95
Trauma	16 (7.58)	9 (7.38)/7 (7.87)	7.04
Macrocephaly/ventriculomegaly w/o associated CNS abnormality	11 (5.21)	5 (4.10)/6 (6.74)	8.06
Dandy-Walker malformation/obstructive arachnoid cyst	9 (4.26)	5 (4.10)/4 (4.49)	5.95
Postnatal meningitis	8 (3.79)	5 (4.10)/3 (3.37)	6.95
Craniosynostosis	2 (0.95)	2 (1.64)/0 (0)	1.33
Congenital CNS infection	2 (0.95)	2 (1.64)/0 (0)	8.96
Pseudotumor cerebri	1 (0.47)	1 (0.82)/0 (0)	12.33

CNS = central nervous system.

TABLE 3

Shunt malfunction surgery indications in the SCH population of 211 patients

Indication	No. of Cases (%)
Acute shunt malfunction	179 (81.0)
Presumed shunt infection	31 (14.0)
Disconnected shunt hardware (asymptomatic)	8 (3.6)
Subacute overdrainage symptoms	3 (1.4)
Total	221

TABLE 4

Intraoperative SCH with acute shunt malfunction on 179 occasions

Shunt Type & Findings	No. of Cases (%)
VP shunt	151
Proximal obstruction	81 (53.6)
Valve obstruction/malfunction	10 (6.6)
Distal obstruction	6 (4.0)
Multiple sites of obstruction	7 (4.6)
No clear site of obstruction	28 (18.5)
Proximal malposition	8 (5.3)
Kink in distal tubing	1 (0.7)
Disconnection	10 (6.6)
Ventriculoatrial shunt	16
Cardiac arrhythmia *	1 (6.2)
Proximal obstruction	9 (56.2)
Multiple obstructions	1 (6.2)
No clear site of obstruction	5 (31.2)
Ventriculopleural shunt	4
Pleural effusion	2 (50)
Proximal obstruction	1 (25)
No clear intraop obstruction	1 (25)
Cystoperitoneal shunt	5
Proximal obstruction	2 (40)
Valve obstruction/malfunction	1 (20)
Distal obstruction	1 (20)
No clear intraop obstruction	1 (20)
Subgaleal-peritoneal shunt	3
Proximal obstruction	1 (33.3)
Distal catheter migration	2 (66.7)

* The patient in this case was hemodynamically stable but was experiencing frequent premature ventricular complexes by cardiac telemetry. There was complete resolution of these premature ventricular complexes after the distal (atrial) catheter was shortened by 2 cm.

TABLE 5

Summary of VP shunt ventricular catheters included in statistical analysis

Catheter No.	Patient No.	Patient Age (mos)	Patient Sex	Hydrocephalus Etiology	Time Catheter Implanted (days)	Catheter Make	Primary Cellular Response	Notes
1	1	0.33	M	Myelo	7	Med A	Microglia	
2	2	44	M	IVH	13	Med A	Microglia	
3	3	5	F	IVH	40	Med A	Microglia	
4	4	6	M	IVH	46	Med A	Microglia	
5	5	1	M	AS	23	Med A	Microglia	Microglia response example in Fig. 4
6	6	20	F	Tumor	41	Cod B H	Microglia	
7	7	122	M	AC (quadrigeminal)	3	Med A	Microglia	
8*	8*	151	F	DWV	4	Cod B H	Mixed	
9*	8*	151	F	DWV	4	Cod B H	Mixed	
10	2	33	M	IVH	130	Med A	Mixed	
11	9	10	F	DW	128	Med A	Mixed	
12	10	234	M	IVH	62	Med A	Mixed	
13	11	206	F	AS	13	Med A	Mixed	Secondary attachment of sparse cells w/punctate TTR+ labeling via astrocytes in 5/16 holes imaged
14	12	109	F	IVH (loculated)	64	Med A	Mixed	Secondary attachment of TTR+ cells via astrocytes in 3/16 holes imaged
15	12	110	F	IVH (loculated)	28	Med A	Mixed	
16	12	110	F	IVH (loculated)	1	Med A	Mixed	
17	13	4	M	IVH	12	Med A	Mixed	Mixed response example in Fig. 4
18	14	2.5	M	Myelo	73	Med A	Mixed	Extensive secondary attachment of choroid plexus (Fig. 6)
19	9	6	F	DW	59	Med A	Astrocyte	Example in Fig. 2; secondary attachment of TTR+ cells in 1/16 holes imaged

Catheter No.	Patient No.	Patient Age (mos)	Patient Sex	Hydrocephalus Etiology	Time Catheter Implanted (days)	Catheter Make	Primary Cellular Response	Notes
20	15	153	F	Myelo	8	Cod B H	Astrocyte	
21	16	9	M	IVH	215	Med A	Astrocyte	Secondary attachment of TTR+ cells in 3/16 holes imaged (Fig. 5)
22	17	244	F	Myelo	3873	Cod AF	Astrocyte	Secondary attachment of TTR+ cells in 1/20 holes imaged
23	12	110	F	IVH (loculated)	2312	Med S	Astrocyte	Astrocyte response example in Fig. 4; sparse secondary attachment of TTR+ cells in 1/16 holes imaged
24	18	33	M	AC (suprasellar)	632	Cod B M	Astrocyte	

AC = arachnoid cyst; AS = aqueductal stenosis; Cod AF = Codman Accu-Flo; Cod B H = Codman Bactiseal Holter; Cod B M = Codman Bactiseal Medos; DW = Dandy-Walker; DWV = Dandy-Walker variant; IVH = intraventricular hemorrhage of prematurity; Med A = Medtronic Ares; Med S = Medtronic barium-impregnated ventricular catheter; Myelo = myelomeningocele; TTR+ = TTR positive.

* The 2 catheters received from Patient 8 were implanted and explanted at the same time and demonstrated nearly identical mixed cellular responses and, as such, were tabulated only once for the purposes of statistical analysis.

TABLE 6

Summary of VP shunt ventricular catheters imaged but not included in statistical analysis

Catheter No.	Patient No.	Patient Age (mos)	Patient Sex	Hydrocephalus Etiology	Time Catheter Implanted (days)	Catheter Make	Primary Cellular Response Observed*	Reason for Exclusion From Analysis
25	11	192	F	AS	4198	Cod B M	Mixed	Bugbee
26	7	127	M	AC (quadrigeminal)	147	Med A	Mixed	Bugbee
27	2	43	M	IVH	329	Med A	Mixed	Bugbee
28	19	124	M	Tumor	520	Med A	Astrocyte	Bugbee
29	20	184	F	AC (4th ventricular)	2711	Cod AF	Astrocyte	Bugbee
30	21	200	M	Myelo	172	Med A	Astrocyte	Bugbee (example in Fig. 3)
31	21	194	M	Myelo	92	Med A	Astrocyte	Bugbee
32	8	151	F	DWV	4	Cod B H	Not classifiable	Weak/irregular labeling†
33	22	166	F	AC (4th ventricular)	15	Med A	Not classifiable	Weak/irregular labeling†
34	23	239	F	PM	714	Cod B H	Not classifiable	Weak/irregular labeling†
35	24	53	F	IVH	7	Med A	Not classifiable	Autofluorescence‡
36	6	22	F	Tumor	63	Med A	Not classifiable	Autofluorescence‡

PM = postnatal meningitis.

*Although observed cellular responses for Bugbee wire treated samples are reported, there is significant potential for irregularities in IHC labeling with electrocautery-related protein denaturation.

†These samples all possessed diffuse, weak IHC labeling patterns raising suspicion for poor, inadequate, or excessive fixation; Bugbee wire exposure not documented in the transcribed operative report; and/or errors in sample preparation. Of note, the weakly labeled cell masses visualized on these catheters lacked any identifiable morphological characteristics (that is, not choroid plexus, lymphocytes, neutrophils).

‡It remains unclear why these 2 catheters demonstrated such significant autofluorescence, most pronounced in the 594-nm wavelength channel. Notably, while both of these catheters were barium impregnated, the same catheter make had been successfully imaged on other occasions. As with the catheters demonstrating weak labeling, cells were present on these catheters by virtue of the presence of nuclei, which could be visualized given less pronounced autofluorescence in the lower wavelength channel used to visualize the Hoechst stain.